Int. J. Multiphase Flow Vol. 16, No. 4, pp. 713–725, 1990
Printed in Great Britain.

0301-9322/90 $3.00 + 0.00

PARTICLE TRAJECTORIES NEAR FREELY ROTATING SPHEROIDS IN SIMPLE SHEAR FLOW

J. PETLICKI and T. G. M. VAN DE VEN
Pulp and Paper Research Institute of Canada and Department of Chemistry, McGill University, Montreal, Quebec H3A 2A7, Canada

(*Received* 15 *June* 1989; *in revised form* 15 *February* 1990)

Abstract—Equations to describe the velocity of a spherical particle near a freely rotating spheroid in simple shear flow have been formulated and integrated numerically. Both hydrodynamic and colloidal interactions have been taken into account. Examples are given of trajectories of particles leading to capture in primary or secondary energy minima.

INTRODUCTION

Most of the theoretical literature on the motion and interactions between particles in flowing suspensions deals with spherical particles, in the main with equal ones. Many real flowing systems relevant to industry, medicine, agriculture and other fields consist of at least two types of particles of completely different shape, size and surface properties, interacting hydrodynamically and colloidally. If the particles differ appreciably in size, and the larger ones are more rod- or disk-like than spherical, as, for example, fillers and fibers in papermaking (van de Ven & Mason 1981), it seems to be more accurate to approximate the shape of the larger particles as spheroids.

Adamczyk & van de Ven (1983) described and classified pathlines of the fluid element about a spheroid freely rotating in a simple shear flow. In this paper, in order to make the model more realistic, we have included in the theory hydrodynamic and colloidal interactions between a small (but non-Brownian) spherical particle and a large spheroidal collector. Since the general solution is rather complicated, we also discuss simpler but important particular cases of the general solution. Finally, we present selected particle trajectories.

THEORY

We consider a spheroidal collector (with axis ratio $r_e = a/b$, a being the symmetry semi-axis and b a semi-axis perpendicular to it) which is smooth, rigid and suspended under neutrally buoyant conditions in a viscous Newtonian fluid, subjected to a low Reynolds number simple shear flow.

Relative to a space-fixed Cartesian coordinate frame X' (figure 1) with the origin coinciding with the collector center, the undisturbed flow $\mathbf{v}'$ is taken to be

$$v_i' = \delta_{i3} G x_2', \qquad [1]$$

where δ_{ij} is the Kronecker delta and G the shear rate. We employ particle-fixed Cartesian coordinates X_i (with their origin at the center of the spheroid) with the X_1-axis aligned along the symmetry axis of the spheroid. The transformation from the X-frame to the X'-frame is carried out via the rotation matrix α_{ij},

$$x_i' = \alpha_{ij} x_j, \qquad [2]$$

which itself is defined in terms of the Euler angles θ, ϕ and ψ:

$$\alpha_{ij} = \begin{pmatrix} \cos\theta & -\sin\theta\cos\psi & \sin\theta\sin\psi \\ \sin\theta\cos\phi & -\sin\phi\sin\psi + \cos\theta\cos\phi\cos\psi & -\sin\phi\cos\psi - \cos\theta\cos\phi\sin\psi \\ \sin\theta\sin\phi & \cos\phi\sin\psi + \cos\theta\sin\phi\cos\psi & \cos\phi\cos\psi - \cos\theta\sin\phi\sin\psi \end{pmatrix}. \qquad [3]$$

The angular velocity $\boldsymbol{\omega}$ of the spheroid relative to the fixed frame X' is

$$\boldsymbol{\omega} = \begin{pmatrix} 0 & -\omega_3 & \omega_2 \\ \omega_3 & 0 & -\omega_1 \\ -\omega_2 & \omega_1 & 0 \end{pmatrix}, \quad [4]$$

where the ω_is are the spins of the spheroid about their respective axes:

$$\omega_1 = \dot{\psi} + \dot{\phi}\cos\theta, \quad [5a]$$

$$\omega_2 = \dot{\theta}\sin\psi - \dot{\phi}\sin\theta\cos\psi \quad [5b]$$

and

$$\omega_3 = \dot{\theta}\cos\psi + \dot{\phi}\sin\theta\sin\psi, \quad [5c]$$

and where $\dot{\theta}$, $\dot{\phi}$ and $\dot{\psi}$ denote the time derivatives of the three Euler angles.

The motion of a spheroid in simple shear in terms of the Euler angles was determined by Jeffery (1922):

$$\dot{\theta} = \tfrac{1}{4}GB\sin 2\theta\sin 2\phi, \quad [6a]$$

$$\dot{\phi} = \tfrac{1}{2}G(1 + B\cos 2\phi) \quad [6b]$$

and

$$\dot{\psi} = -\tfrac{1}{2}GB\cos\theta\cos 2\phi, \quad [6c]$$

where

$$B = \frac{r_e^2 - 1}{r_e^2 + 1}.$$

Equation [6c] gives rise to an elliptic integral, but [6a] and [6b] can be integrated analytically with the result:

$$\tan\theta = C(r_e^2\sin^2\tau + \cos^2\tau)^{1/2} \quad [7a]$$

and

$$\tan\phi = r_e\tan\tau \quad [7b]$$

with

$$\tau = \frac{Gt}{r_e + \dfrac{1}{r_e}} + \tan^{-1}\left(\frac{\tan\phi_0}{r_e}\right), \quad [7c]$$

ϕ_0 being the value of the azimuthal angle at time $t = 0$.

The integration constant C is termed the orbit constant and describes the precession of the symmetry axis of the spheroid about the vorticity axis of the undisturbed flow (X_1'-axis). The orbit constant ranges from C = 0 (the symmetry axis parallel to the undisturbed vorticity) to C = ∞ (the symmetry axis in the plane perpendicular to the undisturbed vorticity).

According to [7b] the motion of a spheroid is periodic, with the period given by

$$T = \frac{2\pi}{G}\left(r_e + \frac{1}{r_e}\right). \quad [8]$$

The spin ω_1 of the spheroid about the symmetry axis X_1 is a simple function of the polar angle θ. Substituting [6b] and [6c] into [5a], one obtains:

$$\omega_1 = \frac{G}{2}\cos\theta. \quad [9]$$

Thus, the spheroid spins with constant angular velocity $\omega_1 = G/2$ when C = 0 and does not spin when C = ∞. Additionally, from [7a–c] and [9] it follows that for C $\in \langle 0, \infty \rangle$ the spin of prolate spheroids ($r_e > 1$) is maximal for aximuthal angles $\phi = n\pi$, where $n = 0, 1, 2\ldots$ (i.e. when the spheroid is oriented across the stream), and minimal in the aligned position when $\phi = (1/2 + n)\pi$. For oblate spheroids the opposite is true.

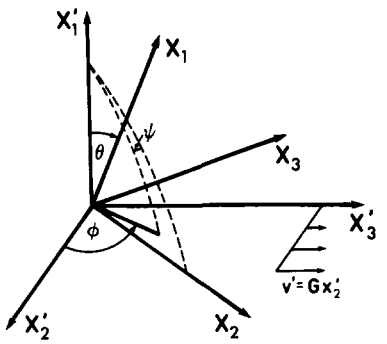

Figure 1. Particle fixed coordinate frame X relative to space fixed coordinate system X'. The X_1-axis coincides with the symmetry axis of the spheroid; θ, ϕ and ψ are the three Euler angles.

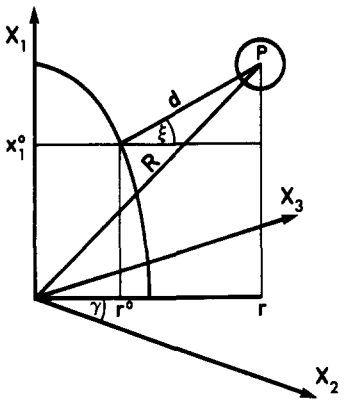

Figure 2. Cross section of one quadrant of the spheroid in the plane determined by the center of the particle $P(x_1, x_2, x_3)$ and the projection r of the position vector $\mathbf{R}$ on the X_2X_3-plane. γ and ξ are angles appearing in matrix [17].

The equations of motion [6a–c] were deduced by Jeffery (1922) from the flow field about a spheroid arbitrarily oriented, but instantaneously fixed relative to the X'-frame. Since the no-slip boundary condition at the spheroid surface is assumed, Jeffery's fluid velocity field $\mathbf{v}^J$ must be transformed to one rotating with the spheroid frame X. This transformation can be expressed as (Adamczyk & van de Ven 1983)

$$\mathbf{v} = \mathbf{v}^J - \boldsymbol{\omega} \times \mathbf{R}, \qquad [10a]$$

where $\mathbf{R}$ is the position vector and $\mathbf{R}^2 = x_1^2 + x_2^2 + x_3^2$. The complete expressions for $\mathbf{v}^J$ are given in the appendix.

In general, the flow field near the spheroid is changing periodically in time with a period equal to the period of rotation of the spheroid T and depends on the orbit constant C. Moreover, the instantaneous velocity vector $\mathbf{v}$ depends on the orientation of the spheroid in space and the fluid element position relative to the spheroid surface.

For a spheroid with its symmetry axis aligned along the vorticity axis in the undisturbed linear shear flow (orbit constant C = 0), the flow field becomes simplified and after transformation of [10a] to the fixed Cartesian frame X', the flow can be expressed as (see the appendix):

$$v_i' = Gx_2'\delta_{i3} - \frac{G}{2\alpha_0'}\left[\frac{2\lambda P^2 x_i' x_2' x_3'}{(1+\lambda)^4(r_e^2+\lambda)^{1/2}} + \alpha'(x_2'\delta_{i3} + x_3'\delta_{i2})\right], \qquad [10b]$$

where λ is the spheroidal coordinate (see the appendix),

$$\frac{1}{P^2} = \frac{x_1'^2}{(r_e^2+\lambda)^2} + \frac{x_2'^2 + x_3'^2}{(1+\lambda)^2} \qquad [11]$$

and

$$\alpha' = \int_\lambda^\infty \frac{d\lambda}{(1+\lambda)^3(r_e^2+\lambda)^{1/2}}; \qquad [12]$$

α_0' denotes the same integral as the one for α', but with the lower limit equal to 0. In this particular case the flow field is in a steady state and the velocity vector $\mathbf{v}$ depends on the orientation of the fluid element relative to the spheroid surface only. For a sphere ($r_e = 1$) the expression [10b] is the same as given by Cox *et al.* (1968).

Let us next consider a rigid spherical particle in the neighborhood of a spheroidal collector and which is small compared to the spheroid. Far from the spheroid the particle center moves with velocity $\mathbf{v}$, but in the vicinity of the collector the particle velocity is different because of particle–collector hydrodynamic and colloidal interactions. The instantaneous fluid velocity $\mathbf{v}$ at the center of the particle can be decomposed into a simple shear and a stagnation point flow. For these particular cases the creeping flow solutions for a sphere near a plane are known as functions of the normal distance between the particle center and the collector surface (Brenner 1961; Goren & O'Neill 1971; Goldman *et al.* 1967).

In the rotating frame the instantaneous normal distance d (cf. figure 2) lies in a plane which is determined by the center of the particle and the projection r of the position vector $\mathbf{R}$ on the X_2X_3-plane, thus reducing the problem to a two-dimensional one. The normal distance can be calculated by solving the equations of the line normal to the ellipse in the point (x_1^0, r^0) and of the surface of the ellipse:

$$r_e \frac{x_1 - x_1^0}{x_1^0} - \frac{r - r^0}{r^0} = 0 \qquad [13]$$

and

$$\frac{x_1^{02}}{a^2} + \frac{r^{02}}{b^2} = 1. \qquad [14]$$

The distance d then equals

$$d = [(x_1 - x_1^0)^2 + (r - r^0)^2]^{1/2}, \qquad [15]$$

where

$$r = (x_2^2 + x_3^2)^{1/2}. \qquad [16]$$

We employ the transformation matrix β_{ij}:

$$\beta_{ij} = \begin{pmatrix} \cos\gamma & -\sin\gamma\cos\xi & -\sin\gamma\sin\xi \\ \sin\gamma & \cos\gamma\cos\xi & \cos\gamma\sin\xi \\ 0 & -\sin\xi & \cos\xi \end{pmatrix} \qquad [17]$$

with

$$\sin\gamma = \frac{x_3}{r}, \quad \sin\xi = \frac{x_1 - x_1^0}{d}$$

and

$$\cos\gamma = \frac{x_2}{r}, \quad \cos\xi = \frac{r - r^0}{d}.$$

It can be shown that β_{ij} transforms the instantaneous velocity components of the fluid element in the center of the particle v_i from the local Cartesian coordinates connected with the rotating frame X to a frame in which the velocity component v_2'' is normal to the spheroid surface and the components v_1'' and v_3'' are parallel to the surface of the spheroid, v_1'' being in the X_1r-plane.

From the components v_i'' near the collector the particle velocity $\mathbf{u}$ can be found from (Adamczyk *et al.* 1983)

$$u_1'' = F_3 v_1'', \qquad [18a]$$

$$u_2'' = F_1 F_2 v_2'' + u_{\text{coll}} \qquad [18b]$$

and

$$u_3'' = F_3 v_3'', \qquad [18c]$$

F_i being the universal hydrodynamic correction functions tabulated by Brenner (1961), Goldman *et al.* (1987) and Goren & O'Neill (1971) and u_{coll} is the velocity due to colloidal forces.

The functions F_i were approximated by the following expressions (Dabros *et al.* 1977):

$$F_1 = \frac{H}{H+1}, \qquad [19a]$$

$$F_2 = \frac{2.23(H+1) - H}{(H+1)^2} \qquad [19b]$$

and

$$F_3 = K\left[1 - \frac{5}{16(H+1)^3}\right], \qquad [19c]$$

with $K = 1$ for $H > 0.3$ and $K = 1.13 + 0.08 \ln H$ for $10^{-6} < H < 0.3$. Here $H = h/a_p$ is the gap width normalized by the particle radius a_p. The maximum deviation of these expressions from the tabulated values is about 5%.

The velocity of the particle due to colloidal forces F_{coll}, which can be derived from interaction energies (Hogg *et al.* 1966; Wiese & Healy 1969), can be expressed as follows:

$$u_{coll} = \frac{F_1 F_{coll}}{6\pi\mu a_p}, \qquad [20]$$

$$F_{coll} = F_{attr} + F_{el}, \qquad [21]$$

$$F_{attr} = -\frac{Aa_p}{6h^2}\left[\frac{1+3.54p}{(1+1.77p)^2}\right] \quad \text{for } p < 1$$

$$= -\frac{Aa_p}{6h^2}\left(\frac{0.98}{p} - \frac{0.434}{p^2} + \frac{0.0674}{p^3}\right) \quad \text{for } p > 1 \qquad [22]$$

and

$$F_{el} = \frac{\pi}{4}\varepsilon\varepsilon_0\kappa a_p \frac{2\zeta_1\zeta_2 - (\zeta_1^2+\zeta_2^2)\exp(-\kappa h)}{\sinh(\kappa h)}, \qquad [23]$$

where F_{attr} and F_{el} are van der Waals attraction forces and the electrostatic forces due to double-layer interactions, A is the Hamaker constant, μ and ε are viscosity and dielectric constant, respectively, of the suspending fluid, ε_0 is the permittivity of free space, ζ_i are the zeta potentials of the particle and of the collector, κ is the reciprocal double-layer parameter and p is the retardation parameter defined as $p = 2\pi h/\lambda_L$, λ_L being the London wavelength.

The particle velocity components u_i can be expressed as linear combinations of the flow field components v_i and the colloidal velocity u_{coll}:

$$u_1 = [F_3 + \beta_{21}^2(F_1F_2 - F_3)]v_1 + c_2v_2 + c_3v_3 + \beta_{21}u_{coll}, \qquad [24a]$$

$$u_2 = c_2v_1 + [F_3 + \beta_{22}^2(F_1F_2 - F_3)]v_2 + c_1v_3 + \beta_{22}u_{coll} \qquad [24b]$$

and

$$u_3 = c_3v_1 + c_1v_2 + [F_3 + \beta_{23}^2(F_1F_2 - F_3)]v_3 + \beta_{23}u_{coll}, \qquad [24c]$$

where

$$c_1 = \beta_{22}\beta_{23}(F_1F_2 - F_3), \qquad [25a]$$

$$c_2 = \beta_{21}\beta_{22}(F_1F_2 - F_3) \qquad [25b]$$

and

$$c_3 = \beta_{21}\beta_{23}(F_1F_2 - F_3), \qquad [25c]$$

and β_{ij} are elements of the matrix [17].

The particle trajectory can now be found by integrating [24a–c] and [6c] numerically with respect to time.† Both the particle position and the spheroid orientation in space must be specified as initial conditions. Since, by means of [2], the components of the position vector x_i can be transformed in between coordinate frames rotating with the spheroid and fixed in space, the particle trajectories can be calculated in both frames.

RESULTS AND DISCUSSION

Since the theory outlined above is valid for any axis ratio r_e, it also applies to $r_e = 1$, i.e. with it we can calculate relative trajectories between a small and a large sphere. The solution of this problem is known from the literature (Adler 1981) and this case can serve as a limiting example for comparing our theory with literature results. Figure 3 shows a comparison of the minimum separation distance in the equatorial plane between two unequal spheres interacting hydrodynamically in simple shear flow for selected radius ratios calculated by P. M. Adler (private communication) and from our theory with $r_e = 1$. When comparing our results with those of Adler

†A FORTRAN version of the program is available from the authors upon request.

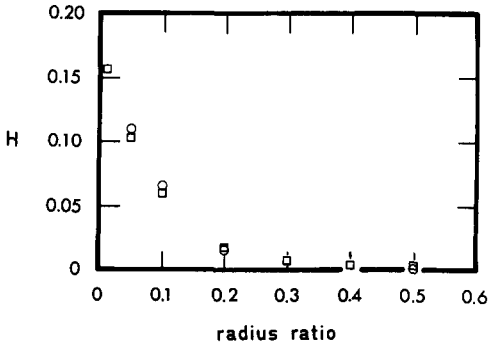

Figure 3. The minimum separation distance in the equatorial plane vs the radius ratio of two unequal spheres interacting hydrodynamically in a simple shear flow. Comparison of the values obtained from sphere–sphere and sphere–plane interaction models: □, sphere near plane; ○, sphere near sphere.

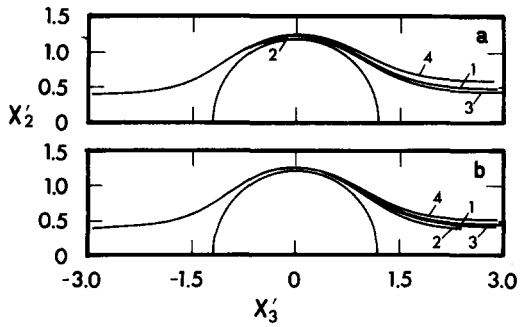

Figure 4. Influence of colloidal forces on the trajectories in the equatorial plane of two unequal spheres in a simple shear flow. The colloidal velocities were calculated using (a) Adler's (1981) and (b) Brenner's (1961) hydrodynamic correction functions. The length scale is normalized by the radius of the larger sphere $b = 5\ \mu$m. Initial position of the particle with $a_p/b = 0.2$: $x_1' = 0$, $x_2' = 0.4$, $x_3' = -3$. Shear rate $G = 100\ s^{-1}$, $\lambda_L = 0.1\ \mu$m, $\mu = 1$ mPa s, $\varepsilon = 80$ and $\zeta_1 = -8.3$ mV. Remaining conditions for A (in 10^{-20} J), κb and ζ_2 (in mV): **1**, (5, 100, −8.3); **2**, (5, 100, 8.3); **3**, (50, 100, −8.3); **4**, (5, 60, −8.3).

(1981), it can be seen that the results of his calculations should be used when the radius ratio exceeds 0.2, but become inaccurate for lower radius radii. Below this limit, the hydrodynamic correction functions F_i approximated by [19a–c] can be used with very good accuracy. The hydrodynamic correction functions F_2 and F_3, for particles which are not very small compared to the large reference sphere, can be estimated from the expressions given by Adler (1981), but in this case the Jeffery (1922) orbit of the spheroid can be significantly perturbed by the presence of the particle. The hydrodynamic correction function F_1 is the ratio of the particle velocity under an applied force normal to the collector surface, and the velocity which the particle would experience in an unbounded fluid under this same force. According to this definition, F_1 must be normalized to one far from a collector surface. However, we noticed that Adler's (1981) correction functions, denoted by C in his paper, are not normalized to one. Figures 4(a, b) show the influence of the colloidal forces on the trajectories. In figure 4(a), the trajectories were calculated for various colloidal forces using Adler's values for F_1. The results are indistinguishable from those given in figure 9 of Adler's (1981) paper, proving that our method is mathematically sound for $r_c = 1$. In figure 4(b), Brenner's (1961) correction function F_1 was used and the results show that the influence of colloidal forces is less significant than suggested by figure 4(a).

The general solution of the particle velocity equations [24a–c] becomes simplified for gap widths h between particle and spheroid surfaces greater than the radius of the particle. From the values of F_i it follows that $F_1 F_2 \approx 1$ when $h > a_p$. The equations of motion [24a–c] can then be reduced to

$$u_i = v_i + \beta_{2i} u_{coll} \qquad [26]$$

and for weak colloidal interactions the particle, for all practical purposes, moves along the fluid pathline, i.e. as a fluid element at its center. Since pathlines about a spheroid were described by Adamczyk & van de Ven (1983), we will focus our attention on the case when the particle has a chance to approach the surface of the spheroid closer than its radius.

In the absence of any repulsive colloidal forces the particle can be captured in the primary energy minimum. From the moment of physical contact the particle velocity relative to the collector surface is equal to zero and the particle moves as a point on the spheroid surface. Generally, these orbits are not closed (cf. figure 5). In the particular case when the particle is captured at the tip of the spheroid, the orbit is closed. For orbit constants C = 0 and C = ∞ the particle moves along a circle.

In the presence of repulsive double-layer interactions, a non-Brownian particle can be permanently captured in the secondary energy minimum if either the shear rate is sufficiently low or the minimum is deep enough. In this case the particle moves relative to the spheroid surface. In the

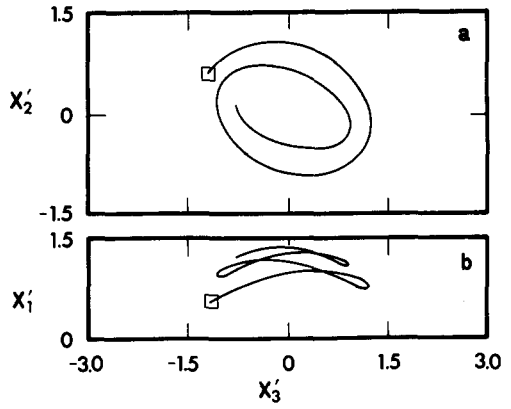

Figure 5. Example of a trajectory of a particle captured in the primary energy minimum. The center of the particle at the moment of capture is marked by □. The length scale is normalized by the spheroid minor semi-axis with $b = 10\,\mu$m and $r_e = 2$. Projections on (a) $X_2'X_3'$- and (b) $X_1'X_3'$-planes. Initial position of the particle with $a_p/b = 0.05$: $x_1' = 0.6$, $x_2' = 0.2$, $x_3' = -22$. Initial spheroid orientation: $\phi_0 = 0$ and C = 1. $G = 1\ s^{-1}$, $\mu = 1$ mPa s, $\varepsilon = 80$, $A = 5 \times 10^{-20}$ J, $\lambda_L = 0.1\,\mu$m and $\zeta_i = 0$.

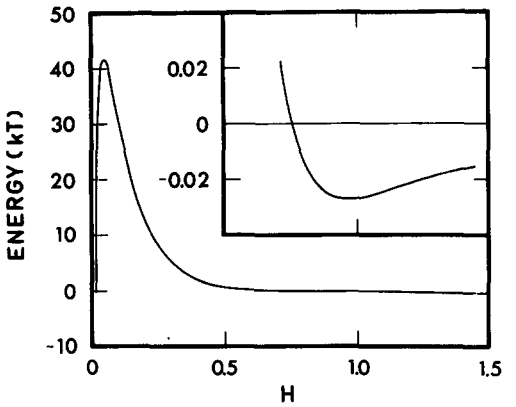

Figure 6. Energy profile and enlargement of the secondary energy minimum (inset) vs dimensionless gap width calculated for: $a_p = 0.5\,\mu$m, $A = 5 \times 10^{-20}$ J, $\zeta_1 = \zeta_2 = -20$ mV, $\kappa = 2 \times 10^7\ m^{-1}$, $\lambda_L = 0.1\,\mu$m, $\mu = 1$ mPa s and $\varepsilon = 80$.

main this motion is tangential but, additionally, the particle oscillates in the energy minimum in the direction normal to the spheroid surface with an amplitude depending on the shape and position of the energy minimum and on the shear rate. In general, for C $\in \langle 0, \infty \rangle$, each particle trajectory consists of three parts: (i) particle approach to the spheroid and its capture in the secondary minimum; (ii) movement along a non-stationary trajectory; and, finally, (iii) motions along the steady-state trajectory.

An example of a trajectory computed for a selected energy barrier (figure 6) is shown in figures 7–9. Figures 7–9(a, b) show the projection of the sphere trajectory on the $X_2'X_3'$- and $X_1'X_3'$-plane,

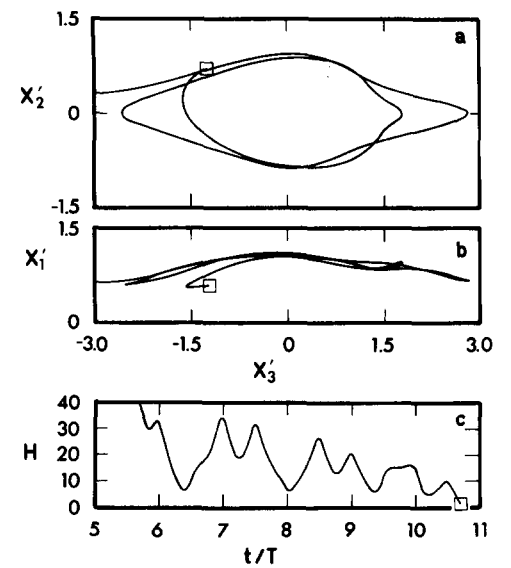

Figure 7. An example of particle approach to the spheroid and its capture in the secondary energy minimum (cf. figure 6) marked by □. (a) and (b)—projections of the trajectory on $X_2'X_3'$- and $X_1'X_3'$-planes, respectively. The length scale is normalized by the minor semi-axis of the spheroid $b = 10\,\mu$m with $r_e = 2$. (c) Dimensionless gap width vs time. Initial position of the particle: $x_1' = 0.6$, $x_2' = 0.2$, $x_3' = -22$. Initial spheroid orientation: $\phi = 0$ and C = 1. $G = 0.01\ s^{-1}$. The remaining parameters are as in figure 6.

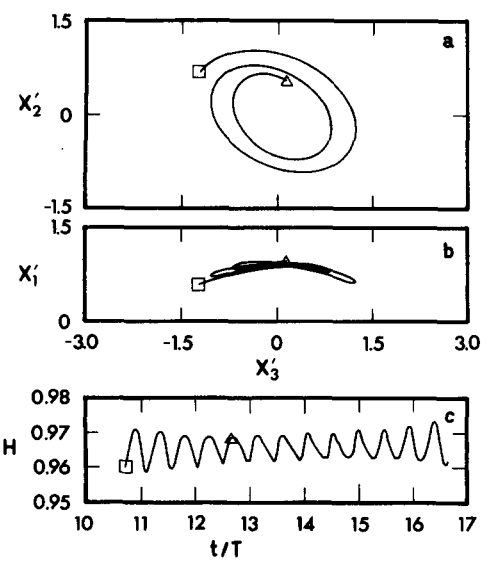

Figure 8. Non-stationary part of the particle trajectory captured in the secondary minimum. Continuation of figure 7 to an arbitrary moment marked by △ (a and b) and beyond (c).

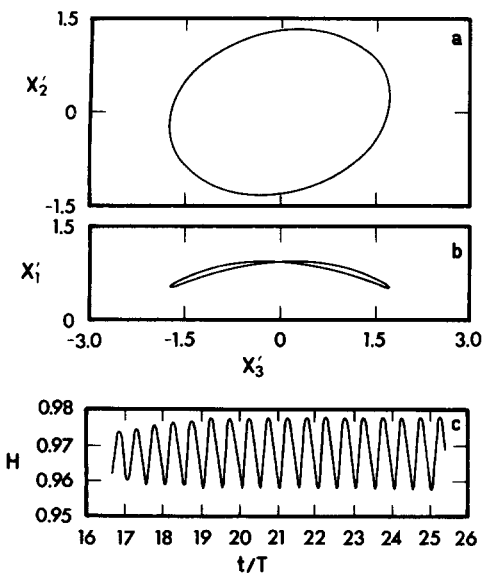

Figure 9. Steady-state trajectory ($t/T \gtrsim 20$) of the particle captured in the secondary energy minimum. Continuation of figures 7 and 8.

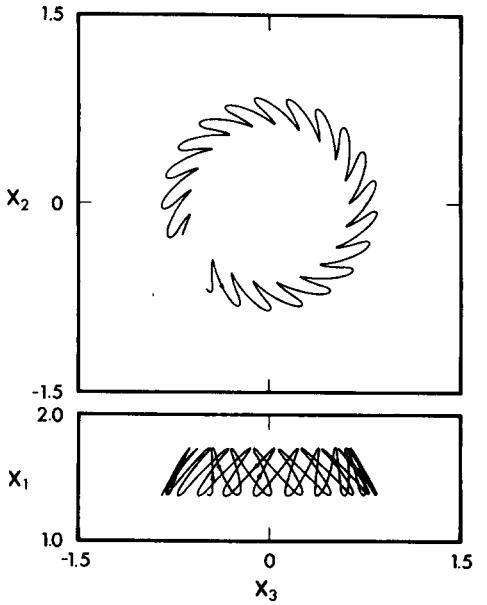

Figure 10. Projections of the steady-state trajectory (cf. figure 9) in frame X rotating with the spheroid.

respectively. Figures 7–9(c) represent variations of the gap width between the particle and the spheroid in time. The time scale (normalized by the period of rotation of the spheroid) can be used to specify the instantaneous orientation of the spheroid in space (cf. [7a–c]). The steady-state part of this trajectory (cf. figure 9) is shown in figure 10 in the rotating frame X.

It is interesting to note that in a particle–solvent–spheroid system for a fixed orbit constant C only two (one above and one below the plane of shear) steady-state trajectories (limit cycles) exist, regardless of the initial particle position and the initial spheroid orientation in azimuthal angle ϕ_0.

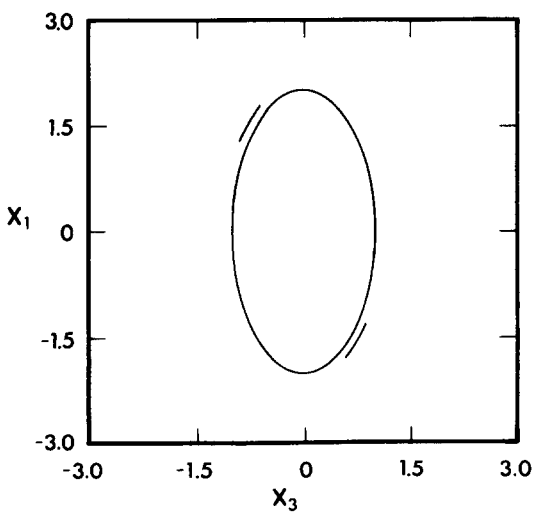

Figure 11. Steady-state secondary minimum trajectories of particles near the sphereoid rotating with C = ∞. Projection in the rotating frame X. The remaining parameters (except the initial particle position: $x_1' = 0.3$, $x_2' = 0.3$, $x_3' = \pm 22$) as in figures 6 and 7.

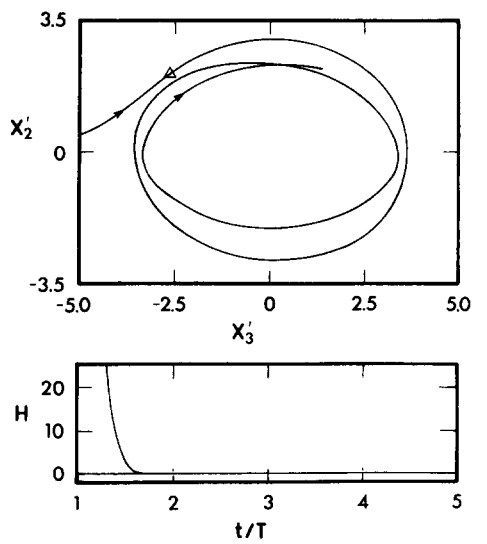

Figure 12. Example of direct capture of a particle during the first encounter. Projection of the trajectory on $X_2'X_3'$-plane and dimensionless gap width vs time. Moment of capture is marked by △. The length scale is normalized by the minor semi-axis of the spheroid with $b = 5\,\mu$m and $r_e = 5$. Initial particle orientation with $a_p/b = 0.2$: $x_1' = 0.4$, $x_2' = 0.33$, $x_3' = -22$. Shear rate $G = 1\,\text{s}^{-1}$, $\mu = 1$ mPa s, $\varepsilon = 80$, $A = 5 \times 10^{-20}$ J, $\lambda_L = 0.1\,\mu$m and $\zeta_i = 0$. Initial spheroid orientation: C = 1 and $\phi_0 = 90°$.

In the particular case C = 0, only one trajectory exists which is nearly circular in the equatorial plane. A particle arriving at the spheroid away from the equatorial plane will slowly approach this limit cycle while orbiting the spheroid, due to a tangential velocity component caused by the curvature of the spheroid. For C = ∞, there are two trajectories and the particle motion is two-dimensional in the X_2X_3-plane. The latter case is shown in figure 11 in the coordinate frame X, rotating with the spheroid. Of course the trajectories presented here are possible only in ideal systems in which particles are ideally smooth and uniform and a spheroid rotates exactly according to Jeffery's (1922) equations of motion. Since steady-state conditions are reached only after many periods of rotation their experimental verification in real systems can be rather problematic.

The non-stationary part of a trajectory for a particle captured in a secondary minimum and the particle trajectory rotating with a spheroid (cf. figures 8 and 5) can be very similar. Differentiation between them is rather difficult since a particle moves slowly relative to a spheroid surface and oscillates with an amplitude not exceeding a few percent of its radius. Moreover, these oscillations and the thermal motion of particles usually overlap.

From the infinite number of initial spheroid orientations in the azimuthal angle ϕ_0, it follows that the trajectory equations [24a–c] have an infinite number of solutions. In considering the transport of particles to the spheroidal collector, the state which will be reached by a particle after one or more encounters with a spheroid seems to be more important than the shape of its trajectory. We have identified five possible states: (i) direct capture; (ii) simple separation; (iii) delayed capture; (iv) delayed separation; and (v) capture in the flow field. State (i) is reached when a particle is immediately captured by a spheroid during the first encounter (cf. figure 12). State (ii) is defined by a single-pass trajectory (cf. figure 13). In states (iii) and (iv), a particle orbits a spheroid one or many times and in the end is captured (figure 14) or separates towards infinity (figure 15). Sometimes it is impossible to differentiate between states (iii) and (iv) in a reasonable amount of computation time. Thus we employ state (v), in which a particle is captured in the flow field about a spheroid (cf. figure 16). The probability that the particle reaches these states depends mainly on the orbit constant of the spheroid and its period of rotation. It is important to note that all the trajectories shown in figures 12–16 were selected for the same initial position of the particle and orbit constant of the spheroid: the only difference was the value of ϕ at $t = 0$.

CONCLUDING REMARKS

In this paper we presented the solution for the particle velocity field near a spheroid freely rotating in a simple shear flow and we compared it with previously presented solutions for two unequal-sized spheres.

From our general solution we concluded that a spherical particle moves almost unperturbed along a pathline when the gap width between the particle and the spheroid is greater than the

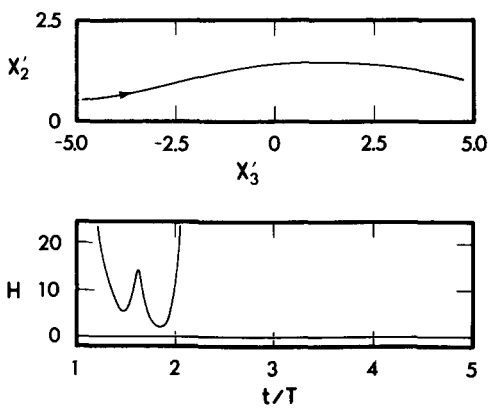

Figure 13. Example of simple separation. $\phi_0 = 100°$. Remaining parameters as in figure 12.

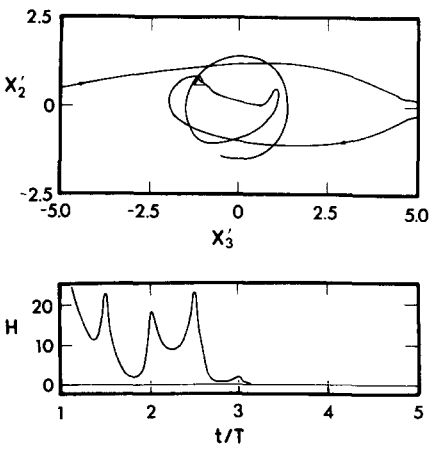

Figure 14. Example of delayed capture. $\phi_0 = 155°$. Moment of capture marked by △. Remaining parameters as in figure 12.

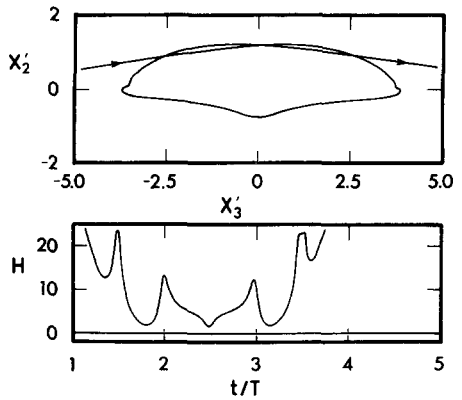

Figure 15. Example of delayed separation (transient orbit). $\phi_0 = 200°$. Remaining parameters as in figure 12.

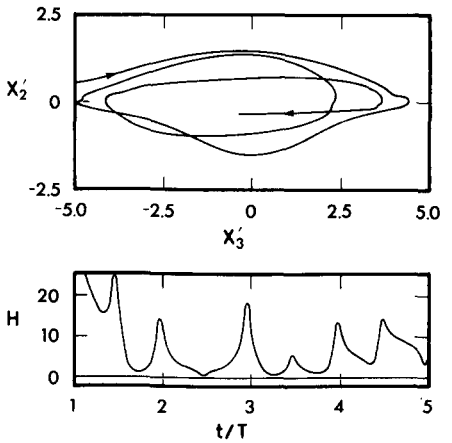

Figure 16. Example of capture in the flow field. $\phi_0 = 50°$. Remaining parameters as in figure 12.

particle radius. When the orbit constant $C = 0$, the flow field, [10a], is qualitatively the same as that for a sphere and only in this particular case does there exist a surface separating open from closed trajectories (van de Ven 1982). For a spheroid rotating with $C > 0$ the situation is much more complicated. Even if particles cross the same point in the undisturbed linear shear flow, the number of possible trajectories is infinite since, even for a fixed orbit constant, an infinite number of spheroid orientations exist with respect to the azimuthal angle ϕ. Therefore, particles approaching the spheroid from the same location can be captured, separated to infinity after an encounter, orbit a spheroid one or more times and eventually be captured or separated. The probability of finding each of the above four situations depends (besides the initial location of the particle) on the orbit constant and the period of rotation of the spheroid. This last conclusion follows from our Monte-Carlo calculations, the results of which will be presented in a forthcoming publication.

For sphere–spheroid systems in which a secondary minimum exists, capture in such a minimum results in stable limit cycles, the shape and location of which depend (besides the magnitude of the colloidal forces) on the orbit constant.

Acknowledgements—The authors wish to thank Dr R. G. Cox for valuable comments and criticism. This work has been supported by the Natural Science and Engineering Council of Canada through Strategic Grant No. G1677.

REFERENCES

ADAMCZYK, Z. & VAN DE VEN, T. G. M. 1983 Pathlines around freely rotating spheroids in simple shear flow. *Int. J. Multiphase Flow* **9,** 203–217.

ADAMCZYK, Z., DABROS, T., CZARNECKI, J. & VAN DE VEN, T. G. M. 1983 Particle transfer to solid surfaces. *Adv. Colloid Interface Sci.* **9,** 183–252.

ADLER, P. M. 1981 Interaction of unequal spheres. I. Hydrodynamic interaction: colloidal forces. *J. Colloid Interface Sci.* **84,** 461–474.

BRENNER, H. 1961 The slow motion of a sphere through a viscous fluid towards a plane surface. *Chem. Engng Sci.* **16,** 242–251.

COX, R. G., ZIA, I. Y. Z. & MASON, S. G. 1968 Particle motions in sheared suspensions. XXV. Streamlines around cylinders and spheres. *J. Colloid Interface Sci.* **27,** 7–18.

DABROS, T., ADAMCZYK, Z. & CZARNECKI, J. 1977 Transport of particles to a rotating disc surface under an external force field. *J. Colloid Interface Sci.* **62,** 529–541.

GOLDMAN, A. J., COX, R. G. & BRENNER, H. 1967 Slow motion of a sphere parallel to a plane wall. Part I. Motion through a quiescent liquid. Part II. Couette flow. *Chem. Engng Sci.* **22,** 637–652; 653–600.

GOREN, S. L. & O'NEILL, M. E. 1971 On the hydrodynamic resistance to a particle of a dilute suspension when in the neighbourhood of a large obstacle. *Chem. Engng Sci.* **26,** 325–338.

HOGG, R., HEALY, T. W. & FUERSTENAU, D. W. 1966 Mutual coagulation of colloidal dispersions. *Trans. Faraday Soc.* **62,** 1638–1651.

JEFFERY, G. B. 1922 The motion of ellipsoidal particles immersed in a viscous fluid. *Proc. R. Soc.* **A102,** 161–179.

VAN DE VEN, T. G. M. 1982 Interactions between colloidal particles in simple shear flow. *Adv. Colloid Interface Sci.* **17,** 105–127.

VAN DE VEN, T. G. M. & MASON, S. G. 1981 Comparison of hydrodynamic and colloidal forces in paper machine headboxes. *Tappi* **40,** 171–175.

WIESE, G. R. & HEALY, T. W. 1969 Effect of particle size on colloid stability. *Trans. Faraday Soc.* **66,** 490–499.

APPENDIX

In this appendix all variables are made dimensionless by division or multiplication by the appropriate combination of variables (G, b, μ).

Jeffery's (1922) solution of the creeping flow equations

$$\nabla^2 \mathbf{v}^J - \nabla p = 0$$

and

$$\nabla \cdot \mathbf{v}^J = 0, \qquad [A.1]$$

with boundary conditions

$$v_1^J = \omega_2 x_3 - \omega_3 x_2,$$

$$v_2^J = \omega_3 x_1 - \omega_1 x_3$$

and

$$v_3^J = \omega_1 x_2 - \omega_2 x_1,$$

at the surface

$$\frac{x_1^2}{r_e^2} + x_2^2 + x_3^2 = 1$$

and

$$v_i^J = D_{ij} x_j$$

far from the surface, where

$$D_{ij} = \begin{pmatrix} \alpha_{21}\alpha_{31} & \alpha_{22}\alpha_{31} & \alpha_{22}\alpha_{31} \\ \alpha_{21}\alpha_{32} & \alpha_{22}\alpha_{32} & \alpha_{23}\alpha_{33} \\ \alpha_{21}\alpha_{33} & \alpha_{22}\alpha_{33} & \alpha_{23}\alpha_{33} \end{pmatrix},$$

α_{ij} being elements of the matrix [3] can be expressed in terms of the spheroidal coordinate λ, which is the positive root of

$$\frac{x_1^2}{r_e^2 + \lambda} + \frac{x_2^2 + x_3^2}{1 + \lambda} = 1, \qquad [A.2]$$

in the following form (Adamczyk & van de Ven 1983; Jeffery 1922):

$$v_1^J = x_1\{\alpha_{21}\alpha_{31} - [\beta'' + 2(\beta - r_e^2\beta')]\mathscr{A}\} + x_2(\alpha_{22}\alpha_{31} - r_e^2\beta'\mathscr{H}) + x_3(\alpha_{23}\alpha_{31} - r_e^2\beta'\mathscr{G})$$
$$- \frac{2\lambda P^2 x_1}{(r_e^2 + \lambda)\Delta}\left[\mathscr{R} - \frac{x_2^2}{(1+\lambda)^2}(\mathscr{B} - \mathscr{A}) - \frac{x_3^2}{(1+\lambda)^2}(2\mathscr{A} + \mathscr{B})\right], \qquad [A.3a]$$

$$v_2^J = x_1(\alpha_{21}\alpha_{32} - \beta'\mathscr{H}) + x_2[\alpha_{22}\alpha_{32} + (\alpha' - r_e^2\beta')\mathscr{A} - (2\alpha'' + \beta'')\mathscr{B}] + x_3(\alpha_{23}\alpha_{32} - \alpha'\mathscr{F})$$
$$- \frac{2\lambda P^2 x_2}{(1+\lambda)\Delta}\left[\mathscr{R} - \frac{x_1^2}{(r_e^2 + \lambda)^2}(\mathscr{B} - \mathscr{A}) - \frac{x_3^2}{(1+\lambda)^2}(2\mathscr{B} + \mathscr{A})\right] \qquad [A.3b]$$

and

$$v_3^J = x_1(\alpha_{21}\alpha_{33} - \beta'\mathscr{G}) + x_2(\alpha_{22}\alpha_{33} - \alpha'\mathscr{F}) + x_3[\alpha_{23}\alpha_{33} + (\alpha'' + \beta'' + \beta - r_e^2\beta')\mathscr{A} + (2\alpha'' + \beta'')\mathscr{B}]$$
$$- \frac{2\lambda P^2 x_3}{(1+\lambda)\Delta}\left[\mathscr{R} + \frac{x_1^2}{(r_e^2+\lambda)}(2\mathscr{A} + \mathscr{B}) + \frac{x_2^2}{(1+\lambda)^2}(2\mathscr{B} + \mathscr{A})\right]. \qquad \text{[A.3c]}$$

Here

$$\mathscr{R} = \frac{1}{1+\lambda}\left(\frac{x_2x_3}{1+\lambda}\mathscr{F} + \frac{x_1x_2}{r_e^2+\lambda}\mathscr{G} + \frac{x_1x_2}{r_e^2+\lambda}\mathscr{H}\right), \quad \mathscr{A} = \frac{\alpha_{21}\alpha_{31}}{3\beta_0''},$$

$$\mathscr{B} = \frac{\beta_0''(2\alpha_{22}\alpha_{32} - \alpha_{23}\alpha_{33}) - \alpha_0''\alpha_{21}\alpha_{31}}{3\beta_0''(2\alpha_0'' + \beta_0'')}, \quad \mathscr{F} = \frac{\alpha_{22}\alpha_{33} + \alpha_{23}\alpha_{32}}{2\alpha_0},$$

$$\mathscr{G} = \frac{\alpha_{23}\alpha_{31} + \alpha_{21}\alpha_{33}}{\beta_0'(r_e^2+1)}, \quad \mathscr{H} = \frac{\alpha_{21}\alpha_{32} + \alpha_{22}\alpha_{31}}{\beta_0'(r_e^2+1)}$$

and

$$\frac{1}{P^2} = \frac{x_1^2}{(r_e^2+\lambda)^2} + \frac{x_2^2+x_3^2}{(1+\lambda)^2}.$$

Moreover,

$$\alpha = \int_\lambda^\infty \frac{d\lambda}{(r_e^2+\lambda)\Delta} = q - \frac{2}{s(r_e^2+\lambda)^{1/2}},$$

where

$$q = \frac{2}{s^{3/2}}\left[\frac{\pi}{2} - \tan^{-1}\left(\frac{(r_e^2+\lambda)^{1/2}}{s^{1/2}}\right)\right] \quad \text{if } r_e < 1$$

$$= \frac{1}{s^{3/2}}\ln\left[\frac{(r_e^2+\lambda)^{1/2} + s^{1/2}}{(r_e^2+\lambda)^{1/2} - s^{1/2}}\right] \quad \text{if } r_e > 1,$$

$$\beta = \int_\lambda^\infty \frac{d\lambda}{(1+\lambda)\Delta} = \frac{1}{\Delta} - \frac{\alpha}{2},$$

$$\alpha' = \int_\lambda^\infty \frac{d\lambda}{(1+\lambda)^2\Delta} = \frac{\Delta}{2s(1+\lambda)^3} - \frac{3\beta}{4s},$$

$$\beta' = \int_\lambda^\infty \frac{d\lambda}{(r_e^2+\lambda)^{1/2}\Delta^2} = \frac{\beta - \alpha}{s},$$

$$\alpha'' = \int_\lambda^\infty \frac{\lambda\, d\lambda}{(1+\lambda)^2\Delta} = \beta - \alpha'$$

and

$$\beta'' = \int_\lambda^\infty \frac{\lambda\, d\lambda}{(1+\lambda)^{1/2}\Delta^2} = \alpha - \beta',$$

with

$$\Delta = (r_e^2+\lambda)^{1/2}(1+\lambda)$$

and

$$s = r_e^2 - 1, \quad s^{1/2} = (|r_e^2 - 1|)^{1/2}.$$

The corresponding integrals with the lower limit of integration replaced by zero are denoted by α_0, α_0', α_0'', β_0, β_0' and β_0''.

For an orbit constant $C = 0$, the matrix [3] reduces to

$$\alpha_{ij} = \begin{pmatrix} 1 & 0 & 0 \\ 0 & \cos(\phi + \psi) & -\sin(\phi + \psi) \\ 0 & \sin(\phi + \psi) & \cos(\phi + \psi) \end{pmatrix},$$

and $\mathscr{A}$, $\mathscr{G}$ and $\mathscr{H}$ are equal to zero. In the space fixed coordinate frame α_{ij} is a unit matrix and, additionally, $\mathscr{B} = 0$ and $\mathscr{F} = (1/2\alpha_0')$. For $C = \infty$, $\mathscr{F}$ and $\mathscr{H}$ are equal to zero.